Check for updates

Ionospheric Response to the Solar Eclipse of August 21, 2017 in Millstone Hill (42N) Observations

Larisa P. Goncharenko[1], Philip J. Erickson[1], Shun-Rong Zhang[1], Ivan Galkin[2], Anthea J. Coster[1], Olusegun F. Jonah[1]

[1]Haystack Observatory, Massachusetts Institute of Technology, 99 Millstone Road, Westford, MA
[2]University of Massachusetts in Lowell, 600 Suffolk St., Lowell, MA

Key Points:

- Observations of ionospheric changes due to the Aug 21, 2017 solar eclipse
- Decrease in electron density by 30-40%, electron temperature by 100-220 K, ion temperature by 50-140 K
- Large 20-40 m/s vertical plasma drift seen in the topside ionosphere during recovery from eclipse is expected to affect plasmasphere

Plain language summary

During the solar eclipse of August 21, 2017, millions of people who watched it from the ground could feel a sudden chill in the air as the moon's shadow moved across the continental US. However, it is far less certain what happens during the solar eclipse in the atmosphere at higher altitudes. Here we present ionospheric observations at 100-600 km above the ground and from > 1000 km away from the totality zone. We report up to 100-140 K cooling in the ion temperature which is very close to the temperature of neutral particles, 100-220 K cooling in electron temperature, and up to 40% reduction in electron density shortly after the maximum obscuration. We suggest that eclipse-induced ionospheric disturbances include a rapid upward flow of plasma from 200 km to much higher altitudes where the plasma is stored and then returned back to lower altitudes several hours after the end of the eclipse. We expect that such effects are stronger closer to the totality zone.

Author Manuscript

This is the author manuscript accepted for publication and has undergone full peer review but has not been through the copyediting, typesetting, pagination and proofreading process, which may lead to differences between this version and the Version of Record. Please cite this article as doi: 10.1029/2018GL077334

Corresponding author: Larisa Goncharenko, lpg@mit.edu

This article is protected by copyright. All rights reserved.

Author Manuscript

Abstract

This study examines the ionospheric changes associated with the solar eclipse of August 21, 2017. The effects associated with the passage of the eclipse shadow were observed more than 1000 km away from the totality at mid-latitudes using the Millstone Hill incoherent scatter radar and digisonde. There was a 30-40% decrease in electron density, a 100-220 K decrease in electron temperature, and a 50-140 K decrease in ion temperature. Surprisingly, the greatest decrease in electron density occurred above 200 km. The most unexpected effect was a large 20-40 m/s upward vertical drift observed in the topside ionosphere right after the local maximum obscuration. We suggest that this drift led to a post-eclipse increase in the topside electron density.

1 Introduction

Observations of ionospheric parameters during solar eclipses present a rare opportunity to examine our state of knowledge about fundamental processes responsible for ionospheric behavior. It is well known that the whole ionosphere, from the *E*, *F1*, and *F2* regions through the topside ionosphere, undergoes dramatic variations at eclipse times due to large changes in solar irradiation. Earlier studies of ionospheric response to solar eclipses consistently show a large decrease in electron density (50-60%) in the *E* and *F1* regions [Salah et al, 1986; Chernyak and Lysenko, 2013]. Changes in *NmE* and *NmF1* are directly proportional to the area of the Sun covered by the Moon [Le et al, 2008], as decreases in solar radiation lead to a decrease in electron production rates. However, *F2*-region ionospheric behavior can be much more complicated, resulting in either a decrease or even a small increase [Muller and Aylward, 1998] in electron density depending on background conditions and onset timing.

While observations of changes in electron density or total electron content during solar eclipses are more widely available in the modern era from networks of ionosondes and GNSS TEC receivers, direct observations of eclipse-induced variations in plasma temperatures and dynamics remain relatively rare. Incoherent scatter radars (ISRs) produce such direct observations due to the radar scattering dependence on plasma temperature, but only a handful of case studies have previously been available due to observational spatial coverage limitations. Evans [1965] reported that in observations with the Millstone Hill ISR during the afternoon eclipse of July 20, 1963, the electron temperature (*Te*) decreased by ~1000 K, while the ion temperature (*Ti*) decreased by 100 K at 350 km and 300 K at 650 km, closely following the solar extreme ultraviolet (EUV) obscuration function. Common ionospheric features reported in prior observations, in particular with ISR measurements, are a marked decrease in electron density (10-60%) and a 100 to 1000 K cooling in electron temperature. In general, the magnitude of ionospheric effects is to first order correlated with the level of EUV obscuration. However, even for a partial eclipse with obscuration of 0.42 under very low solar flux conditions (F10.7 = 66 sfu), ISR eclipse observations have shown a decrease in electron temperature by 100-200 K and a decrease in F-region electron density by 25-30% [Domnin et al, 2013; Chernyak and Lysenko, 2013]. Observations of eclipse effects in the ion temperature are much less consistent, and range from reports of no measurable change [Chernyak and Lysenko, 2013] to a decrease of the order of 40-150 K [Domnin et al, 2013]. Eclipse-induced changes in the vertical drift range from no discernible effect at 200-300 km and ~20 m/s downward drift at 400 km [Salah et al, 1986] to 10-45 m/s downward drift at all F-region altitudes [Domnin et al, 2013]. As changes in vertical drift result from the superposition of three sometimes equal processes - neutral wind forcing, electric field forcing, and ambipolar diffusion - the complicated patterns of observed ionospheric changes provide important condition-dependent information on the different roles of these processes.

This paper uses observations from the Millstone Hill incoherent scatter radar and a co-located digisonde (42.6°N, 288.5°E) to examine the impact of the August 21, 2017

This article is protected by copyright. All rights reserved.

Author Manuscript

solar eclipse on the mid-latitude ionosphere directly above the radar location. We focus only on low-frequency variations (on time scales > ~1.5 hrs) that occur during the eclipse and for several hours after the end of the eclipse. Highlights of the results include a 30-40% decrease in the *F2*-region electron density, a relatively small 100-220 K decrease in electron temperature, and a strong upward drift above the *F2*-region peak following the eclipse.

2 Data and Methods

The Millstone Hill radar operated during August 19-23, 2017 and provided observations prior to, during, and after the solar eclipse. The ISR operation mode was multi-purpose and included cycles alternating zenith pointing, fixed position pointing, and wide regional scans to the south (pointing towards the totality zone). From this comprehensive data set, we concentrate here on vertical ionospheric profiles. Height profiles of ionospheric parameters were sampled with resolution of 4.5 km (best for the *E* and *F1*-region) and 18 km (best for the *F2*-region). The cycling radar mode described above resulted in vertical profile observations at irregular intervals every 7-15 mins. To accurately describe eclipse-induced changes and eliminate influences of TIDs that are omnipresent in observations, we applied a temporal Savitzky-Golay smoothing filter [Savitsky and Golay, 1964] with a 2-degree (parabolic) polynomial over successive 2-hour subsets of data. We note that results remain essentially the same over a wide range of filter window lengths.

Observations by a co-located Millstone Hill digital ionosonde (digisonde) were continuously available during the summer of 2017 with a high temporal resolution (1-2 mins), enabling further investigation of eclipse induced ionospheric changes in a manner complementary to Millstone Hill ISR operations. A 5-min moving mean was applied to digisonde data to highlight essential ionospheric variations.

3 Geophysical conditions

The 21 August 2017 solar eclipse was visible in the continental US, and shadow passage started with a partial eclipse at 16:04 UT over Oregon, ending at 20:10 UT over South Carolina. At the Millstone Hill radar location, a partial solar eclipse was first observed at 17:27 UT (17.45 UT, 12.68 LT) and last observed at 19:59 UT (19.98 UT, 15.22 LT). The maximum solar irradiation obscuration of 62.92% occurred at 18:46 UT (18.77 UT, 14.00 LT), with a magnitude of 0.7. At the time of maximum obscuration over Millstone Hill, the center of totality was located at 33°N and 80°W, and therefore radar vertical profiles sampled the ionosphere directly above the site at a point more than 1000 km to the north-east from totality.

The eclipse occurred during low solar activity, with the solar flux (F10.7) ranging from 86 to 91 SFU (1 SFU = 1E-22 W/m2/Hz) on August 19-23, 2017. This period also experienced minor to moderate geomagnetic activity, with maximum Kp = 4+ to 5 on August 20, Kp = 3 in the early hours of August 21, Kp = 4- to 4+ in the early hours of August 22, and Kp = 5- on August 19 and 23. Although several C class solar flares occurred on Aug 21 and 22, their influence was removed in our analysis through the Savitsky-Golay filtering described above.

In this study we have selected August 22, 2017 as the best available reference to represent the observed state of the non-eclipse ionosphere. To isolate eclipse effects, we also use predictions from the empirical incoherent scatter radar ionospheric model developed from individual ISR long-term observations [Zhang and Holt, 2007].

This article is protected by copyright. All rights reserved.

Author Manuscript

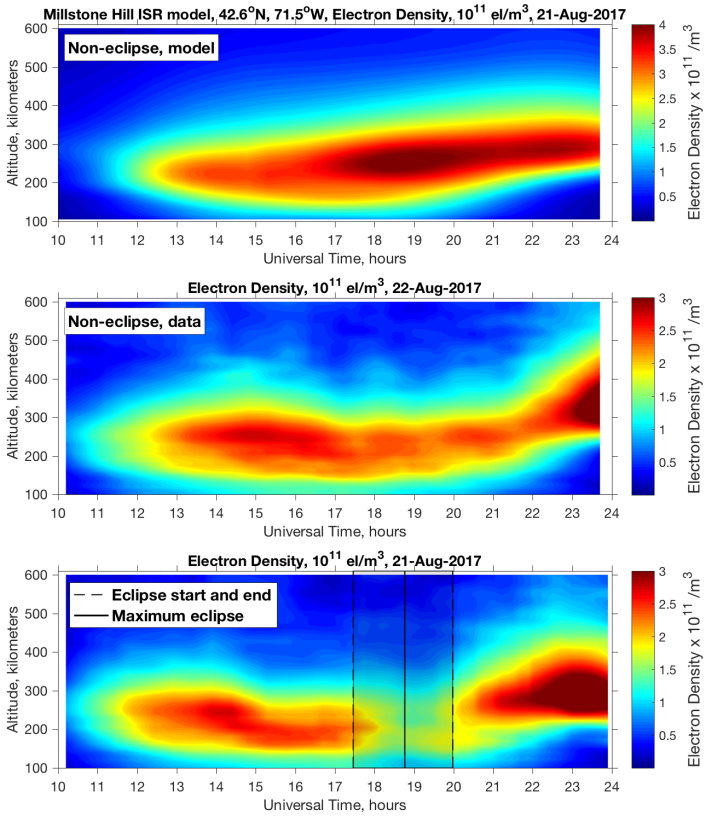

Figure 1. Variations in electron density above Millstone Hill ISR (42.6°N, 288.5°E). (a) predicted by the Millstone Hill empirical model for prevailing solar and geomagnetic conditions, (b) observed on a non-eclipse day, August 22, 2017, and (c) observed during the eclipse on August 21, 2017.

4 Results

A summary of the mid-latitude electron density (*Ne*) vertical observations over Millstone Hill is presented in Figure 1. Figure 1a shows the electron density derived from the Millstone Hill ISR empirical model for these solar and geomagnetic conditions. The main features to note are a post-noon maximum in electron density between ~18-19 UTC and a secondary maximum that occurs in the evening hours, between ~22-24 UTC. This is typical well-known summer behavior that is associated with a combination of variations in thermospheric wind, composition, and solar zenith angle. Figure 1b shows the observations on August 22, 2017, which was selected as the eclipse control (reference) day. It demonstrates several differences from average behavior shown in Figure 1a. First, the overall electron density was lower than the empirical model, likely due to the influence of moderate geomagnetic activity that occurred in the early hours of August 22. Second, the evening maximum was shifted toward later hours (23 to 02 UTC). The evening peak in electron density was also observed at the same time, 23 to 02 UTC, during other days of this campaign (August 19 and 20; not shown), and therefore it is possible that the empirical model does not accurately represent the timing of the evening peak for these conditions. Finally, Figure 1b also shows quasi-periodic fluctuations in *Ne* with scales of the order of 2-3 hours that were superimposed on the smooth diurnal variation in *Ne*. To summarize, the model and non-eclipse day observations predict that, in the absence of

This article is protected by copyright. All rights reserved.

Author Manuscript

eclipse effects, the *F2*-region electron density should have remained at steady levels or somewhat increased in the afternoon hours (17 to 20 UT). Figure 1c shows observations on the eclipse day, with the vertical lines indicating the start, maximum, and the end of the partial eclipse over Millstone Hill. The main eclipse effect was a gradual decrease in electron density at all altitudes from ~100 km to ~600 km, commencing soon after the start of the partial eclipse. This was followed by a quick recovery after the eclipse shadow passage at 20 UTC. The electron density response was altitude-dependent with altitudes < 200 km recovering faster after the maximum eclipse than altitudes above ~250 km, resulting in the peak electron density of the ionosphere being below 200 km. This is expected due to rapid influences of photoionization rate changes on the photochemical equilibrium at these heights.

Figure 2 presents variations in electron temperature (left), ion temperature (center) and vertical plasma drift (right). The electron temperature on Aug 21 and 22 was generally higher than expected, likely due to the lower electron density lowering the electron cooling rate [Roble et al, 1986] and lower heat conduction from the plasmasphere. The eclipse effect was clearly seen as a drop in *Te* at 200-300 km from ~1600-1700 K to ~1500 K shortly after the time of maximum eclipse, at ~19 UT. A decrease in ion temperature was also observed around the time of maximum eclipse, though the magnitude of this decrease was similar to other regularly occurring *Ti* variations (for example, at 14 to 15 UT). The vertical ion drift data reveals some unexpected behavior for summer solar minimum conditions. At altitudes below 200 km, the vertical drift was dominated by the presence of the semidiurnal tide in the lower thermospheric wind system, leading to downward drift in the morning hours (11-13 UT) and upward drift later (15-20 UT). Local sunrise at ~8.5 UT (for 250 km) led to a rapid increase in plasma temperature that produced a strong upward drift above 300 km at 10-12 UT. The daytime drift was generally upward above 350 km, providing a flux of plasma into the plasmasphere, in consistency with earlier observations [Evans , 1971]. All these features were stronger in observations on August 21 and 22 than expected from the empirical model.

To highlight eclipse-related variations in electron density, Figure 3 shows differences in electron density between August 21 and 22, 2017 in absolute (top) and relative percentage (bottom) units. The ~2-3 hr quasi-periodic variations on the control day (Figure 1b) were removed by fitting to a smoothing spline that chosen to minimize edge effects. A decrease in electron density of 0.5-0.99 $\times$ 10^{11} el/m^3 (30-40%) in the F2-region (200-300 km) is seen at the time of the eclipse, with the largest depletion ~8-17 mins after maximum obscuration. Below 200 km, *Ne* decreased by 10-20%. This *Ne* decrease diminished at altitudes above 300 km. Above ~450 km, eclipse-induced variations in general were small and practically not discernible from the background which is subject to large day to day changes. Another remarkable variation seen in Figure 3 was a quick recovery from the eclipse and a large *Ne* increase that commenced soon after the eclipse, peaking at 23-24 UT. A similar post-eclipse increase above the background value was reported in several studies of the August 21, 2017 solar eclipse over many locations across North America [Nayak and Yiğit, 2017; Cherniak and Zakharenkova, 2018; Reinisch et al, 2018; Wu et al, 2018], though the TEC increase is weaker in general as it reflects the integrated *Ne* response over all altitudes. Mechanisms that contribute to a quick recovery and *Ne* increase after 21 UT could include disturbances in the neutral wind and *O/N2* ratio [Muller and Aylward, 1998; Wu et al, 2018].

Eclipse induced changes in mid-latitude electron and ion temperatures and vertical plasma velocity are shown in Figure 4. The electron temperature decreased by 100-220 K during the eclipse, with the coldest temperatures being observed with a 10-20 minutes time lag after the maximum obscuration near the F2-region peak (~220 km) and with ~20-30 minutes time lag at 350 km. A sharp reduction in the electron temperature might be expected due to the decrease in photoelectron heating associated with the reduction in EUV photoionization and the reduction in *Ne*, which linearly reduces the photoelectron

This article is protected by copyright. All rights reserved.

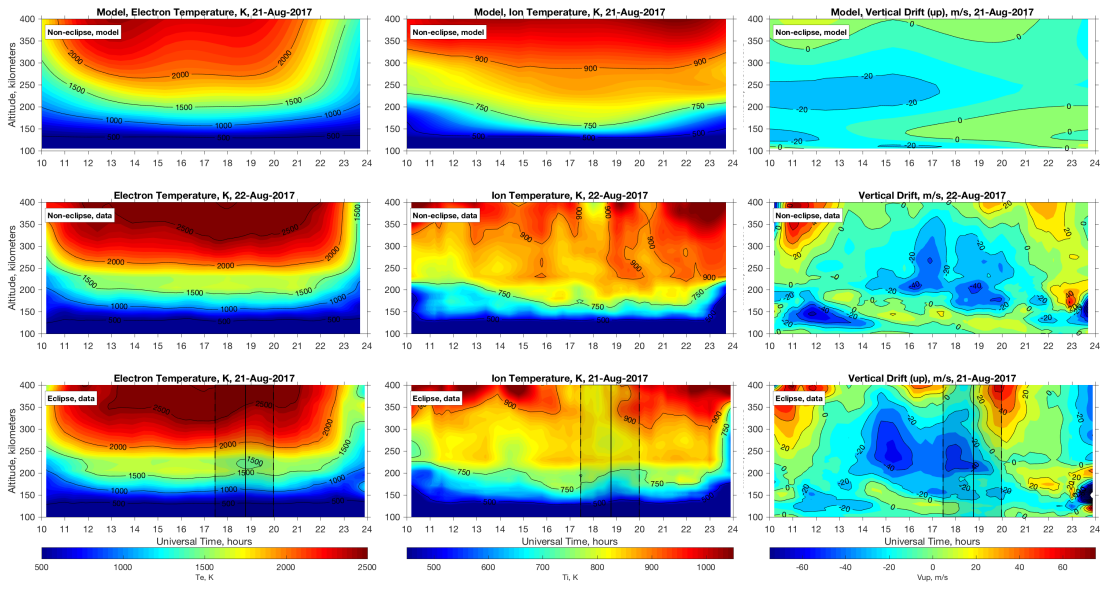

Figure 2. Variations in electron temperature, ion temperature, and vertical drift (positive upward) above Millstone Hill ISR as (top) predicted by the Millstone Hill empirical model, (middle) observed on a non-eclipse day, August 22, 2017, and (bottom) observed during the eclipse on August 21, 2017.

heating. On the other hand, the effect of the decreased heating is opposed by the reduction in thermal electron cooling, which is quadratic in *Ne*. Enhanced downward heat flow from the plasmasphere can also contribute to reduced temperature variations. The magnitude of the 2017 eclipse temperature reduction was much smaller than reported in other eclipse cases at middle latitudes. Earlier studies reported a larger 500-700 K decrease in electron temperature above Millstone Hill for an eclipse with a larger maximum obscuration of 86% [Salah et al, 1986], and even 1000 K decrease for an eclipse with 100% obscuration [Evans, 1965]. It is likely that the large decreases in electron temperature reported for these cases are actually related to the sunset in the conjugate ionosphere.

The 2017 eclipse caused a maximum 70-80 K drop in ion temperature between 250-300 km, centered around the time of maximum obscuration, and a 100-140 K drop in ion temperature at altitudes 150-200 km that lagged behind the time of maximum obscuration. The reduction in ion temperature likely resulted from thermospheric cooling due to the passage of the eclipse shadow and from smaller Coulomb inelastic heat transfer from electrons. A major 100-200 K drop in ion temperature was also observed after the eclipse at 23-24 UT, at the time of a large increase in electron density.

Vertical plasma drift (O+ velocity) during the daytime was generally weakly positive (upward) above ~350 km with magnitudes of 0-15 m/s and negative (downward) at 0-15 m/s between 200-350 km altitude, as seen in Figure 2, in consistency with empirical model and earlier studies [Evans , 1971]. During the eclipse, Figure 4 shows that a 10-15 m/s stronger downward drift was observed between 200-270 km immediately after the start of the eclipse, while there were no measurable changes at higher altitudes. A very strong upward plasma motion with speeds up to 40 m/s higher than normal was observed for ~2 hours after the maximum eclipse (19-21 UTC). The aggregate changes are reminiscent of the effects of a local sunrise, and drift velocities are comparable to velocities observed after the sunrise (see Figure 2). This upward motion could be potentially caused by two contributing factors: (1) immediate (at supersonic speed) ionospheric and thermospheric heating due to recovery from the eclipse, and (2) enhanced southward and

Author Manuscript

This article is protected by copyright. All rights reserved.

Author Manuscript

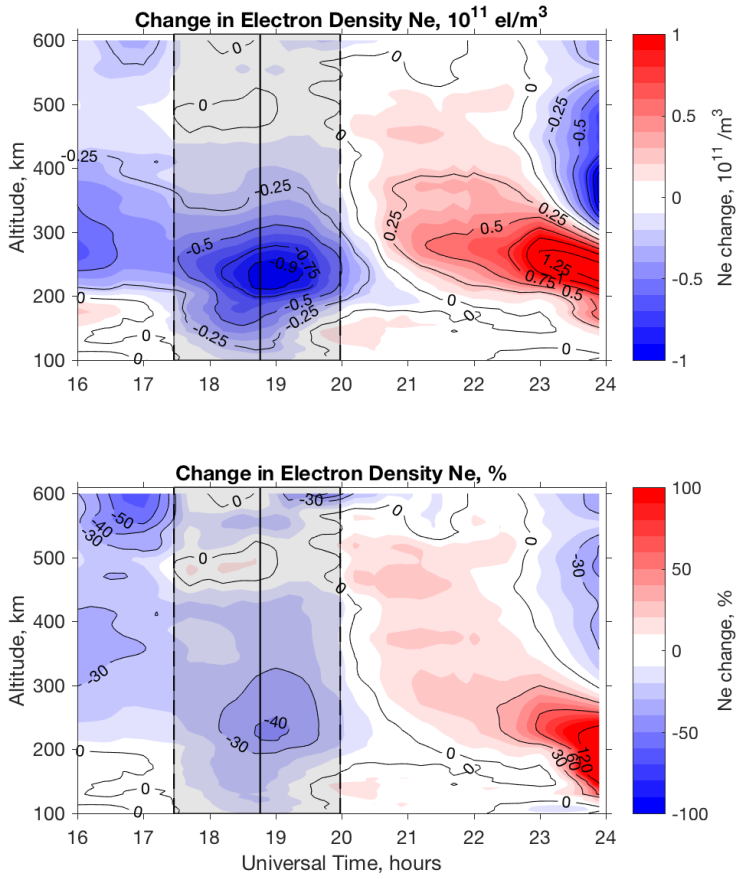

Figure 3. Difference in electron density observed on the eclipse day, August 21, 2017, in comparison with August 22, 2017.

eastward (directed towards maximum shadow) wind as would be anticipated in the eclipse-induced colder thermosphere [Harding et al, 2018].

Upward plasma transport during daytime hours is typically a main source of plasma to the mid-latitude plasmasphere where it can be stored for extended periods of time. Consequently, we expect that topside electron density, initially depleted with eclipse onset, was strongly increased during eclipse recovery following this enhanced upward motion. We also suggest that a large post-eclipse disturbance in *Ne* observed in the evening hours, 21-24 UTC, is one of the primary effects of the eclipse. At 23-24 UT electron density increased by > 50-120% around the peak of the F2-region, but decreased at higher altitudes, as shown in Figure 3. This was also accompanied by a drop in electron and ion temperatures and a strong downward motion as seen in Figure 4. The plasmaspheric flux has a generally positive non-eclipse trend in the daytime and negative at night at Millstone, with a rapid increase observed at this seasonal point in the downward velocity of plasma after opposite hemisphere influence subsides due to conjugate sunset (~23 UTC). A sharp onset of stronger downward vertical velocity and colder plasma temperature at 23 UT, together with an increase in *Ne* by >100%, suggests that the local ionosphere was strongly influenced by the downward influx of cold plasma with anomalously high density from the plasmasphere reservoir, stored there by enhanced diffusive upward flux between 19-21

This article is protected by copyright. All rights reserved.

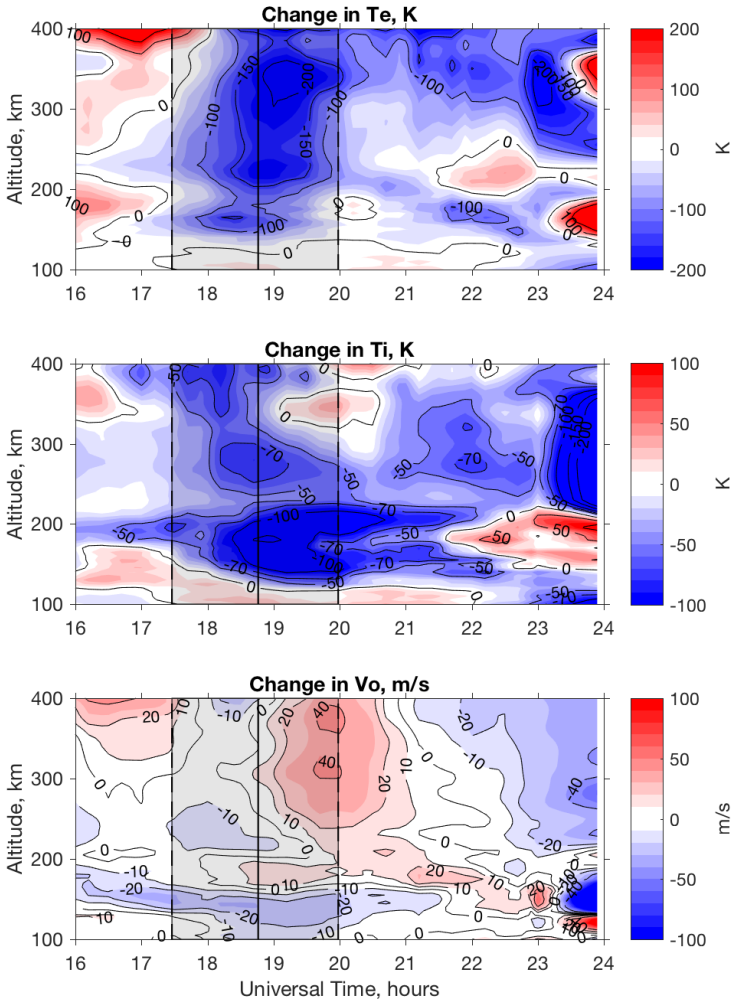

Figure 4. Difference in electron temperature (top), ion temperature (middle), and vertical plasma velocity (bottom) observed on the eclipse day, August 21, 2017. August 22, 2017 is used as control day.

UTC as a result of the solar eclipse recovery. The question is whether such flux exchanges at the topside ionosphere are efficient enough to impact electron density at ionospheric altitudes. Dedicated simulation work as performed in [Reinisch et al, 2018] for the totality zone can provide important insights.

Figure 5 compares digisonde observations of critical frequencies *foF2*, *foF1*, and *foE* and peak heights *hmF2*, *hmF1* and *hmE* during the eclipse day and control day August 22. The main eclipse effect was a rapid decrease in *foF2*, *foF1*, and *foE*, followed by an enhanced post-eclipse *foF2* observed at 21-24 UTC. The magnitude of the eclipse-induced decrease was close to 1 MHz in the *F2* region, ~0.7 MHz in the *F1* region, and ~0.5 MHz in the *E*-region. The start of the decreases occurred almost simultaneously at different altitudes, contrary to earlier observations and simulations. The minimum frequencies were observed with a 2-5 min lag after the maximum obscuration in the *F2* region and very close to the maximum obscuration time at the *F1* region. The *E*-region response

This article is protected by copyright. All rights reserved.

Author Manuscript

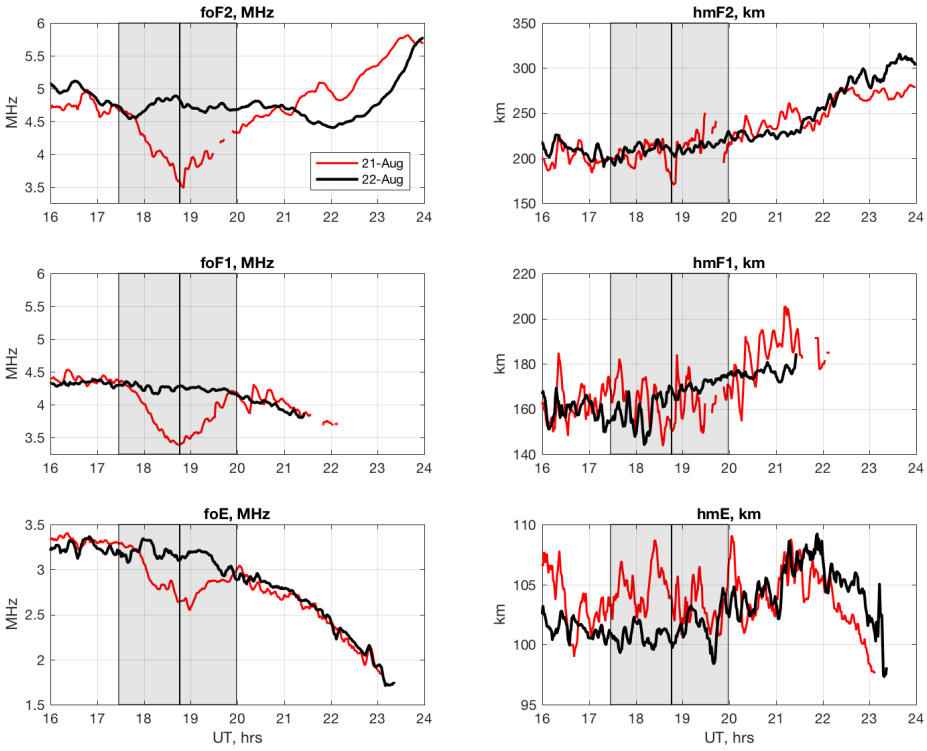

Figure 5. Observations of peak critical frequencies and peak heights of *F2, F1,* and *E* regions by Millstone Hill digisonde on eclipse day August 21, 2017 and control day August 22, 2017. Shaded area indicates the time of partial eclipse on August 21.

seems to have a longer delay than the *F1* region response. This is anomalous because, from consideration of ionization and recombination processes, we expect the *E*-region to respond faster to the eclipse, *F1* region with a short delay, and *F2* region with a longer delay. We note that a C3 solar flare occurred between 17:39 and 17:57 UT, and anomalous behavior described above could be related to the increase in the electron density due to the flare. The timing of the variations observed in the digisonde data also might indicate the presence of strong oscillations in electron density that are superimposed on the eclipse response. In fact, observations of *hmF2*, *hmF1*, and *hmE* indicate such oscillations at all altitudes (Figure 5, right panels) and show that they were stronger on August 21, 2017, started prior to the eclipse, and thus could not be attributed entirely to the eclipse effects. We will address the nature of these oscillations in a separate study.

5 Discussion and summary

This study examines mid-latitude ionospheric variations associated with the solar eclipse on August 21, 2017 using both the Millstone Hill ISR and digisonde, at a location more than 1000 km north-east from the center of totality and with maximum obscuration 63%. Here we summarize the most important features directly observed, some of which present a challenge to current models of the coupled ionosphere and thermosphere.

This article is protected by copyright. All rights reserved.

Author Manuscript

Author Manuscript

1. The state of the ionosphere prior to the eclipse was significantly different than expected for this season and level of solar activity, based on a comparison with Millstone Hill empirical model [Zhang and Holt, 2007]. The electron density was lower by 20-40%, the electron temperature was elevated by 100-450 K, and the ion temperature was decreased by 20-50 K. At least some of these differences were related to the increase in geomagnetic activity for several days prior to the eclipse. In addition, we note the presence of oscillations in all ionospheric parameters with 2-3 hr periods and 20-60 minute periods that constitute typical ionospheric variability and contribute additional 10-25% to variations. Anomalous conditions included a very low (near or below 200 km) *F2* region peak height immediately preceding the eclipse. This preconditioning is expected to influence ionospheric response to the solar eclipse. In our quantitative estimates of eclipse effects, we account for all these factors.
2. The 2017 eclipse caused a 30-40% decrease in electron density, 100-220 K decrease in electron temperature, and 50-140 K decrease in ion temperature. Contrary to simulations [Roble et al, 1986; Ding et al, 2010] and prior observations, the largest decrease in electron density was observed in the F2 region, above 200 km, and not in the F1 region. This was consistent in observation by both instruments, incoherent scatter radar and digisonde. The lowest electron density was observed with a very short time lag after the maximum obscuration, 2-5 mins at 170-200 km and 8-17 mins at ~240 km.
3. The eclipse-induced decrease in electron temperature reached 100-220 K, considerably smaller than 450-1000 K decreases reported in earlier observations [Salah et al, 1986; Chernyak and Lysenko, 2013] and simulations [Roble et al, 1986]. This was possibly related to very low electron density prior to the eclipse and, consequently, low electron cooling rates. The small *Te* reduction was also consistent with the large *Ne* reduction in the *F2* region stated above, as variations in these parameters are anti-correlated and heat content was maintained.
4. In contrast, the decrease in ion temperature during the eclipse reached 100-140 K and was significantly higher than a ~55 K cooling expected from earlier simulations for an eclipse with an even larger solar obscuration rate of 83% [Roble et al, 1986].
5. The most striking observation was a large 20-40 m/s upward plasma drift observed above the *F2* region peak after the maximum obscuration. This upward plasma velocity is similar to effects regularly observed after local sunrise due to associated rapid increases in ionospheric and thermospheric temperature and resulting thermal expansion. To the best of our knowledge, this is the first observational report of eclipse-induced upward transport, as earlier studies reported only downward vertical motion due to the thermospheric cooling. The simulation of Roble et al [1986] indicated a small 2 m/s vertical drift during the eclipse recovery and in a narrow 300-400 km altitude range.
6. A strong upward vertical drift in the topside ionosphere was observed at 19-21 UT, implying an anomalously high upward field aligned diffusion with associated resupply of topside electron density during the daytime hours and subsequent higher downward plasmaspheric flux at nighttime. We hypothesize that a large enhancement in the electron density observed at 21-24 UT as an important eclipse related effect for the August 2017 event.

Acknowledgments

Millstone Hill operations and research at MIT Haystack Observatory are supported by cooperative agreement AGS-1242204 between the US National Science Foundation and the Massachusetts Institute of Technology. For eclipse activities, MIT Haystack was partially supported by NASA grant NNX17AH71G. Millstone Hill ISR data is publicly available

This article is protected by copyright. All rights reserved.

through the Madrigal database at http://madrigal.haystack.mit.edu/madrigal/. Manually scaled digisonde data is available by request from I. Galkin.

References

Cherniak, I. and Lysenko, V., 2013. Measurements of the ionosphere plasma electron density variation by the Kharkov incoherent scatter radar. Acta Geophysica, 61(5), pp.1289-1303.

Cherniak, I., & Zakharenkova, I. (2018). Ionospheric total electron content response to the great American solar eclipse of 21 August 2017. Geophysical Research Letters, 45. https://doi.org/10.1002/2017GL075989.

Ding F., W. Wan, B. Ning, L. Liu, H. Le, G. Xu, M. Wang, G. Li, Y. Chen, Z. Ren, B. Xiong, L. Hu, X. Yue, B. Zhao, F. Li, and M. Yang (2010), GPS TEC response to the 22 July 2009 total solar eclipse in East Asia, J. Geophys. Res., 2010, 115, A07308.

Domnin, I.F., Yemel'yanov, L.Y., Kotov, D.V., Lyashenko, M.V. and Chernogor, L.F., 2013. Solar eclipse of August 1, 2008, above Kharkov: 1. Results of incoherent scatter observations. Geomagnetism and Aeronomy, 53(1), p.113.

Evans, J.V., 1965. An F region eclipse. Journal of Geophysical Research, 70(1), pp.131-142.

Evans, J.V., 1971. Observation of F region vertical velocities at Millstone Hill, 1, Evidence for drifts due to expansion, contraction, and winds. Radio Science, 6(6), pp.609-626.

Harding B. J., D. P. Drob, R. A. Buriti, J. J. Makela, (2018), Nightside detection of a large-scale thermospheric wave generated by a solar eclipse, Geophysical Research Letters, doi: 10.1002/2018GL077015.

Le, H., Liu, L., Yue, X. and Wan, W., 2008, The ionospheric responses to the 11 August 1999 solar eclipse: observations and modeling. In Annales Geophysicae (Vol. 26, No. 1, pp. 107-116). Copernicus GmbH.

Muller-Wodarg, I. C. F., A. D. Aylward, and M. Lockwood (1998), Effects of a mid-latitude solar eclipse on the thermosphere and ionosphere - A modelling study, Geophys. Res. Lett., 25(20), 3787-3790, doi:10.1029/ 1998GL900045.

Nayak, C. and Yiğit, E. (2017). GPS-TEC observation of gravity waves generated in the ionosphere during 21 August 2017 total solar eclipse. Journal of Geophysical Research: Space Physics, 122. https://doi.org/10.1002/2017JA024845

Reinisch, B. W., Dandenault, P. B., Galkin, I. A., Hamel, R., Richards, P. G. (2018), Investigation of the electron density variation during the 21 August 2017 solar eclipse. Geophysical Research Letters, 45, 1253-1261. https://doi.org/10.1002/2017GL076572

Roble, R.G., Emery, B.A. and Ridley, E.C., 1986. Ionospheric and thermospheric response over Millstone Hill to the May 30, 1984, annular solar eclipse. Journal of Geophysical Research: Space Physics, 91(A2), pp.1661-1670.

Salah, J. E., et al. (1986), Observations of the May 30, 1984, annular solar eclipse at Millstone Hill, Journal of Geophysical Research: Space Physics 91.A2 (1986): 1651-1660.

Savitzky, A., and Golay, M. J. E. (1964). Smoothing and differentiation of data by simplified least squares procedures. Analytical Chemistry, 36, 1627-1639.

Wu, Chen, A. J. Ridley, L. Goncharenko, G. Chen, 2018. GITM-Data Comparisons of the Depletion and Enhancement during the 2017 Solar Eclipse. Geophysical Research Letters, doi: 10.1002/2018GL077409.

Zhang, S.R. and Holt, J.M., 2007. Ionospheric climatology and variability from long - term and multiple incoherent scatter radar observations: Climatology in eastern American sector. Journal of Geophysical Research: Space Physics, 112(A6).

Author Manuscript

This article is protected by copyright. All rights reserved.

Figure1.

Author Manuscript

This article is protected by copyright. All rights reserved.

Author Manuscript

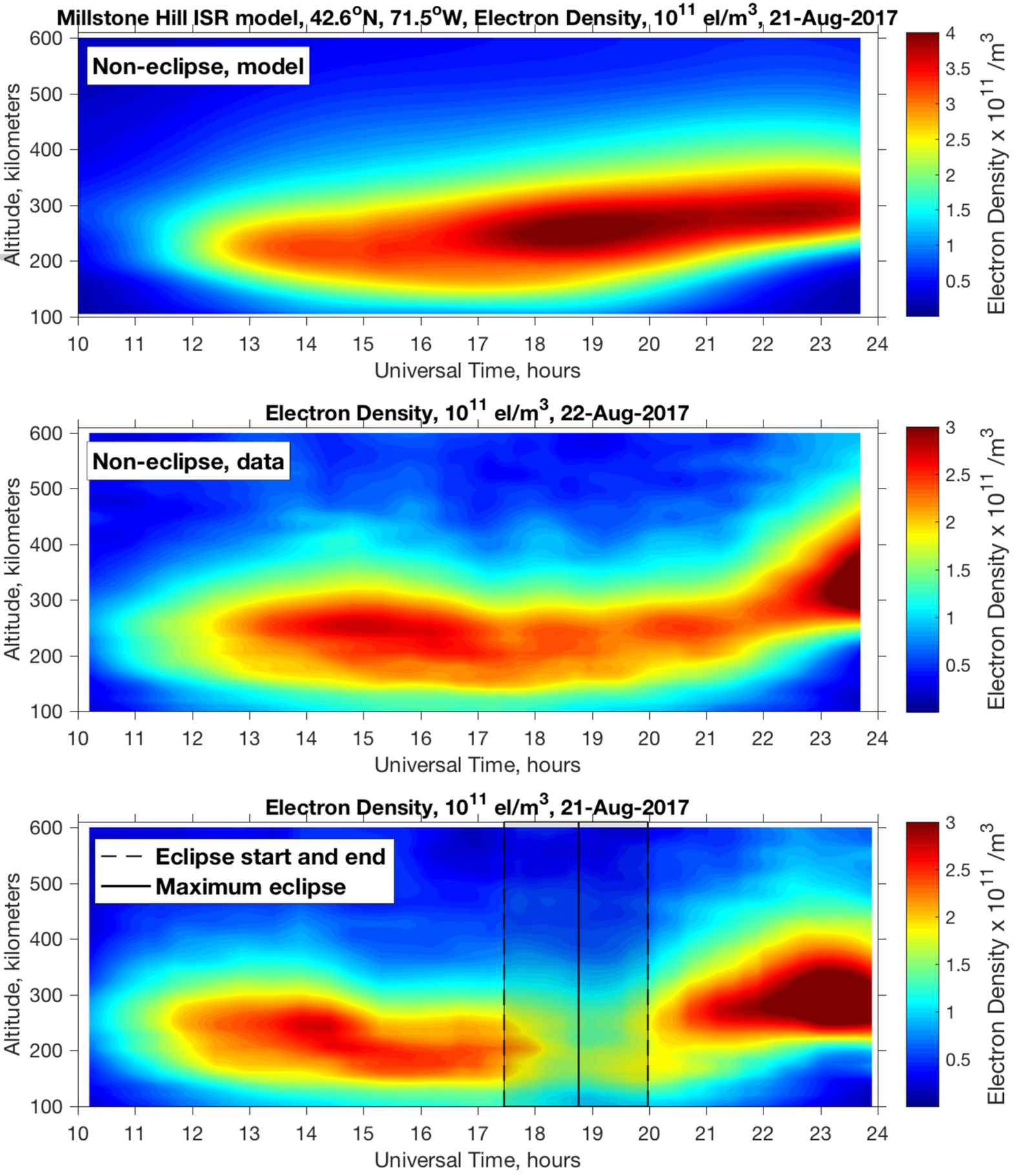

This article is protected by copyright. All rights reserved.

Figure2.

Author Manuscript

This article is protected by copyright. All rights reserved.

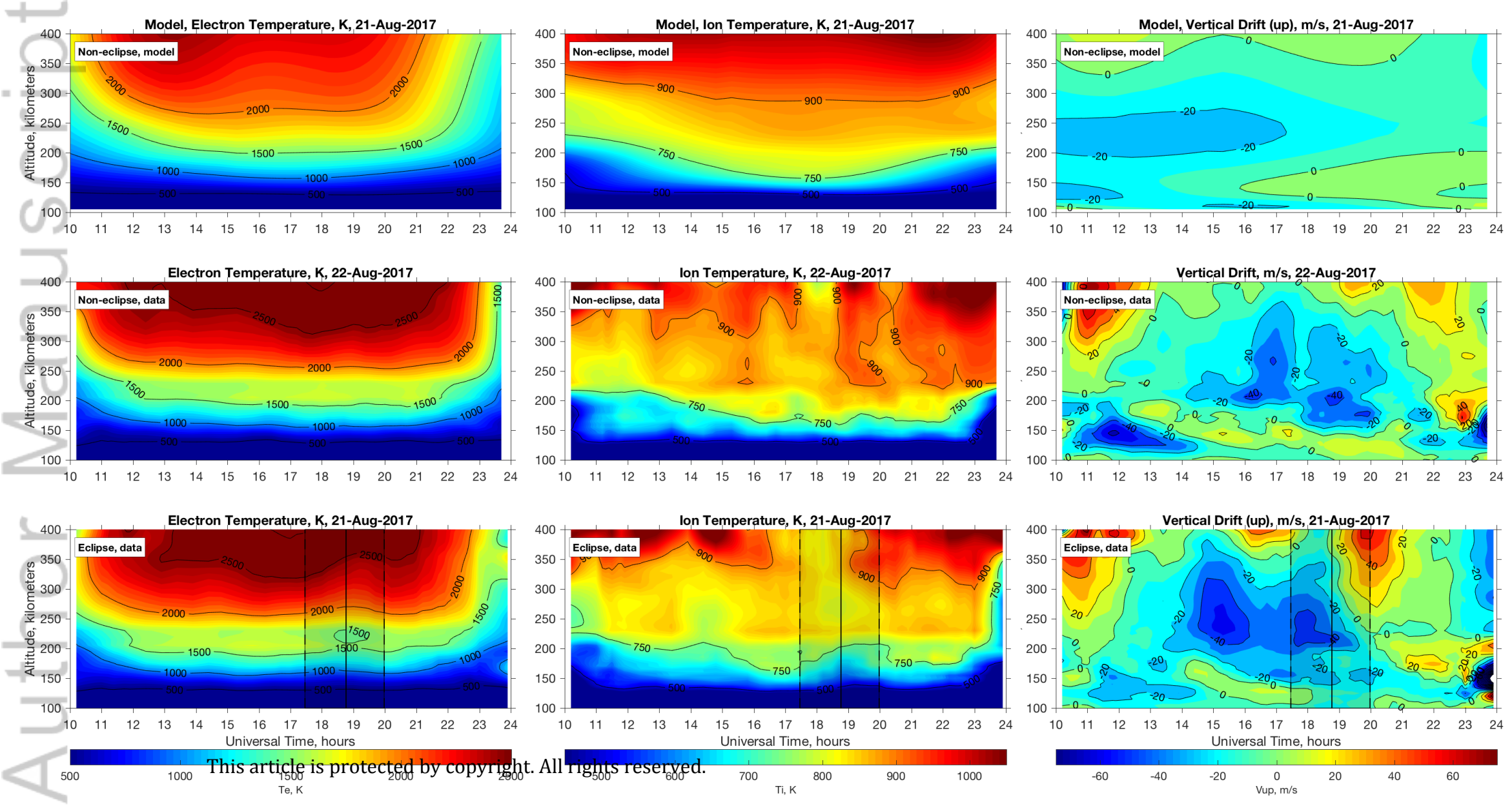

This article is protected by copyright. All rights reserved.

Figure3.

Author Manuscript

This article is protected by copyright. All rights reserved.

Author Manuscript

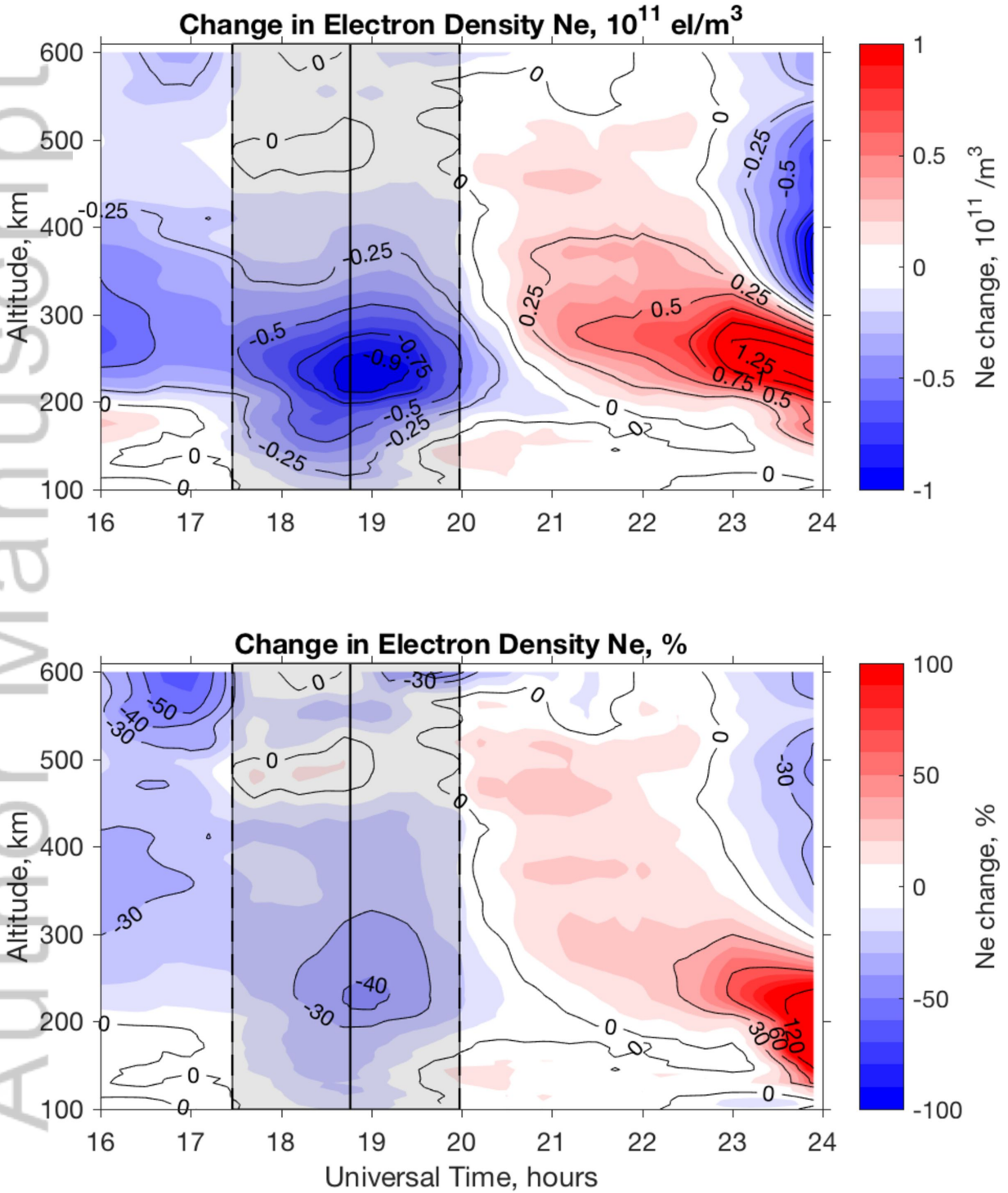

This article is protected by copyright. All rights reserved.

Figure4.

Author Manuscript

This article is protected by copyright. All rights reserved.

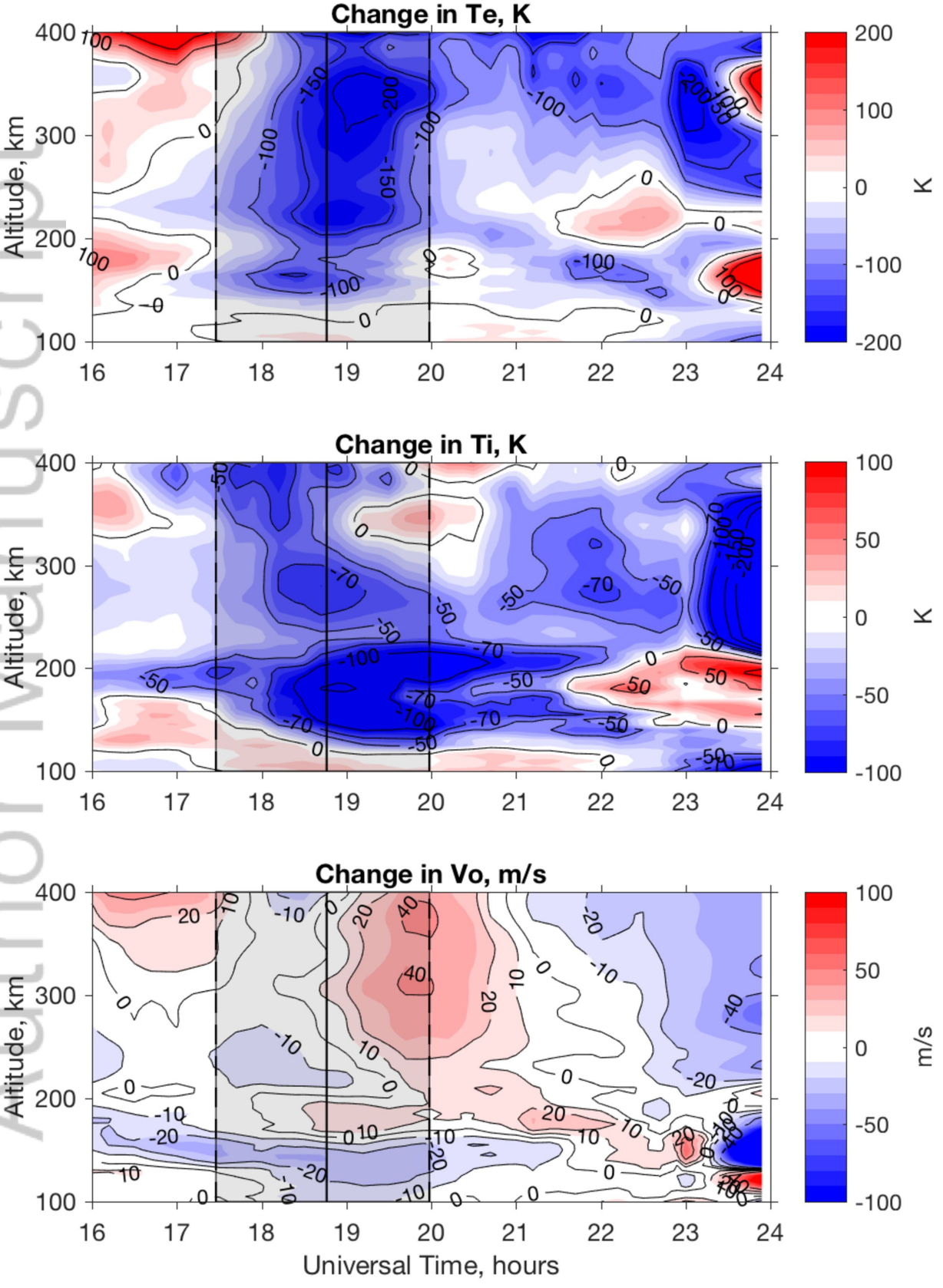

Author Manuscript

This article is protected by copyright. All rights reserved.

Figure5.

Author Manuscript

This article is protected by copyright. All rights reserved.

Author Manuscript

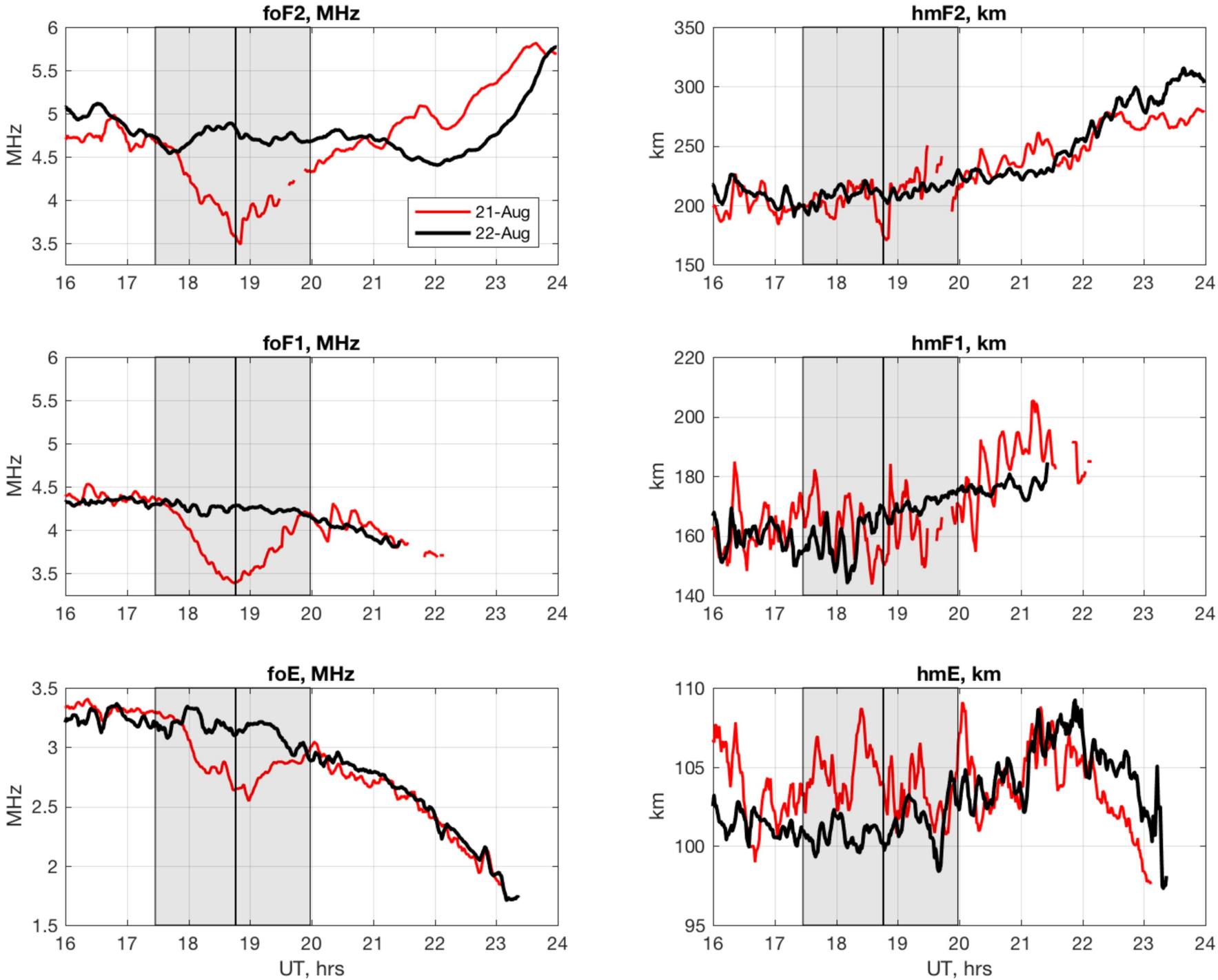

This article is protected by copyright. All rights reserved.

Author Manuscript

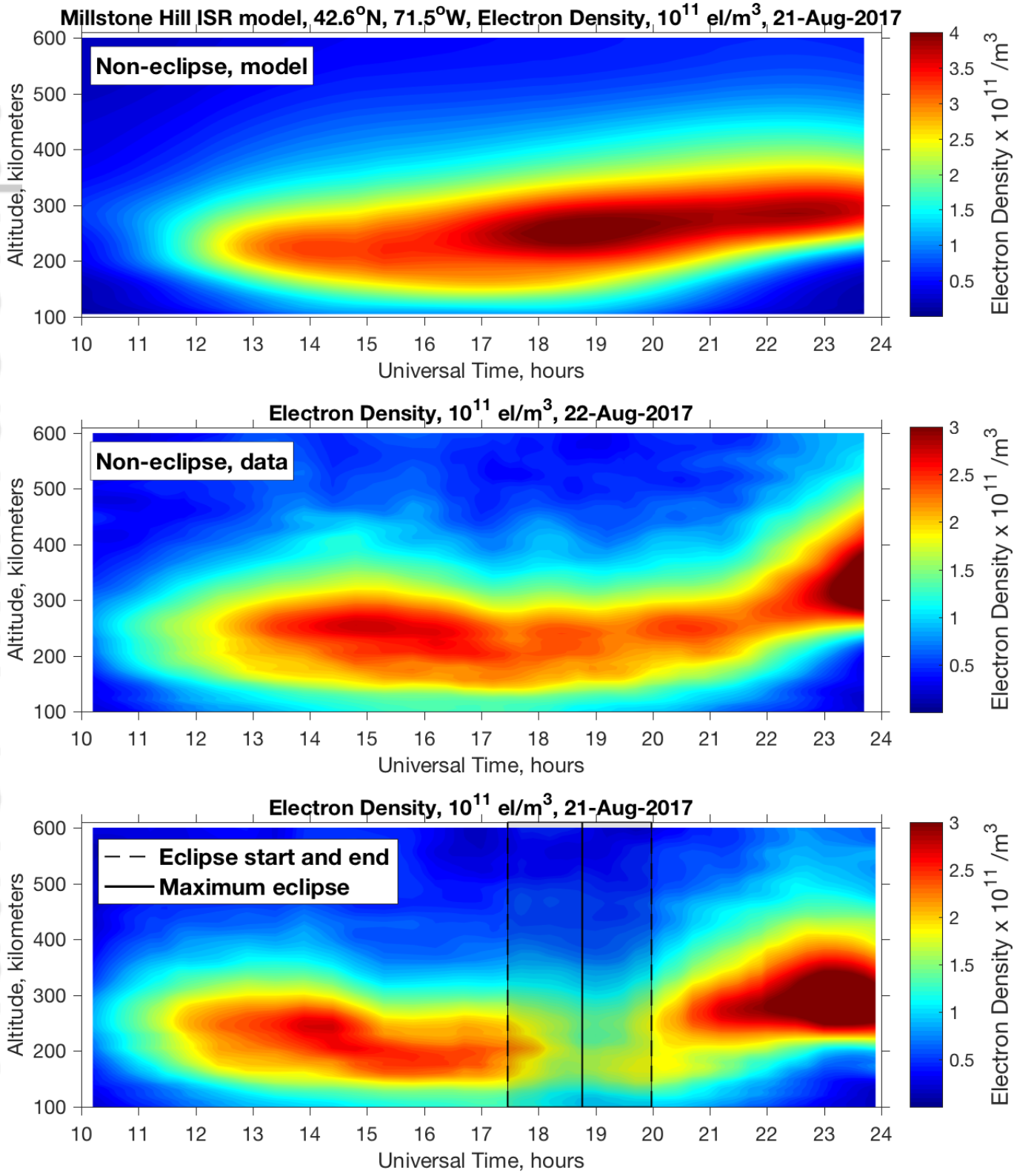

2018GL077334-f01-z-.png

This article is protected by copyright. All rights reserved.

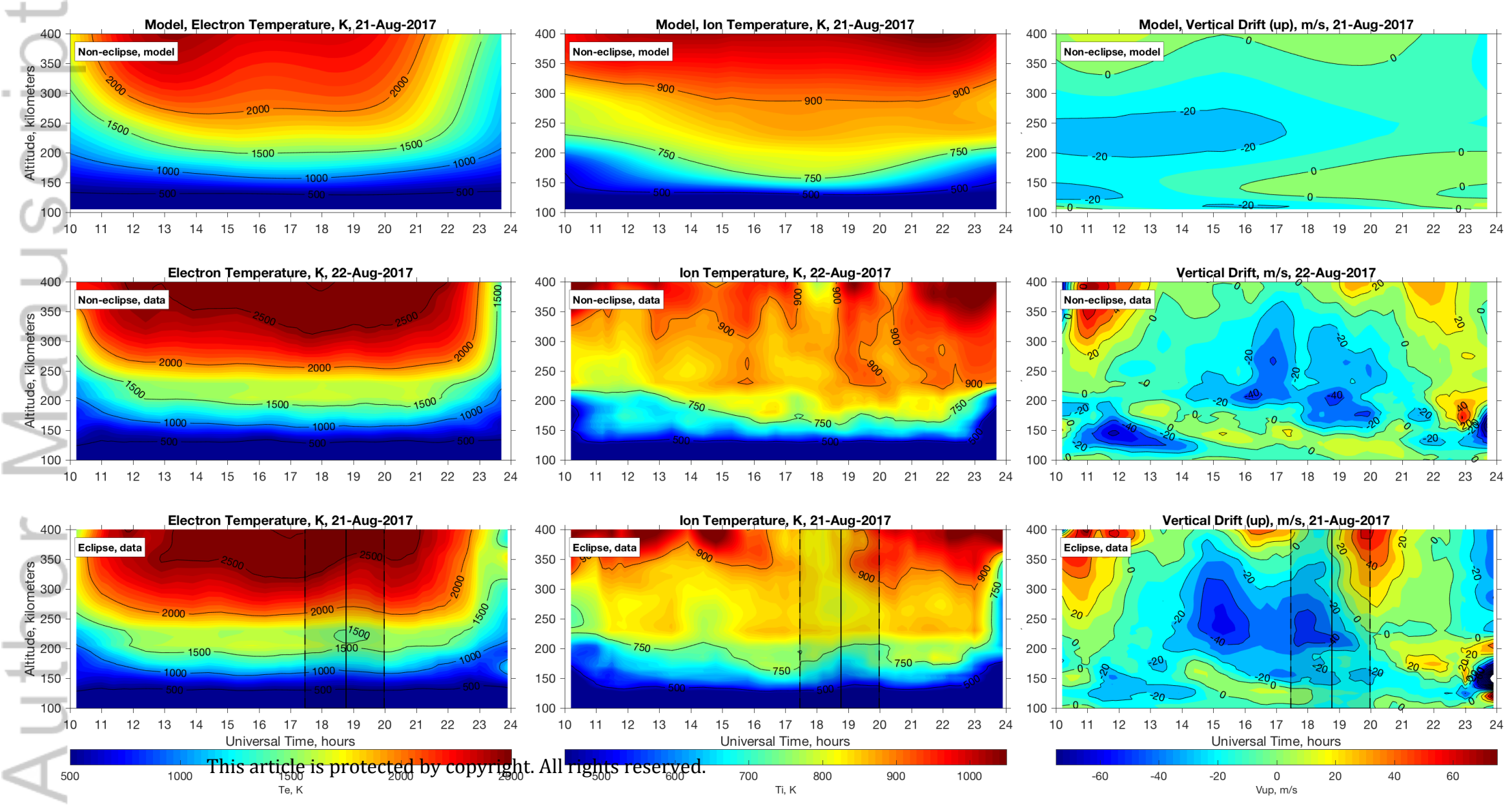

This article is protected by copyright. All rights reserved.

Author Manuscript

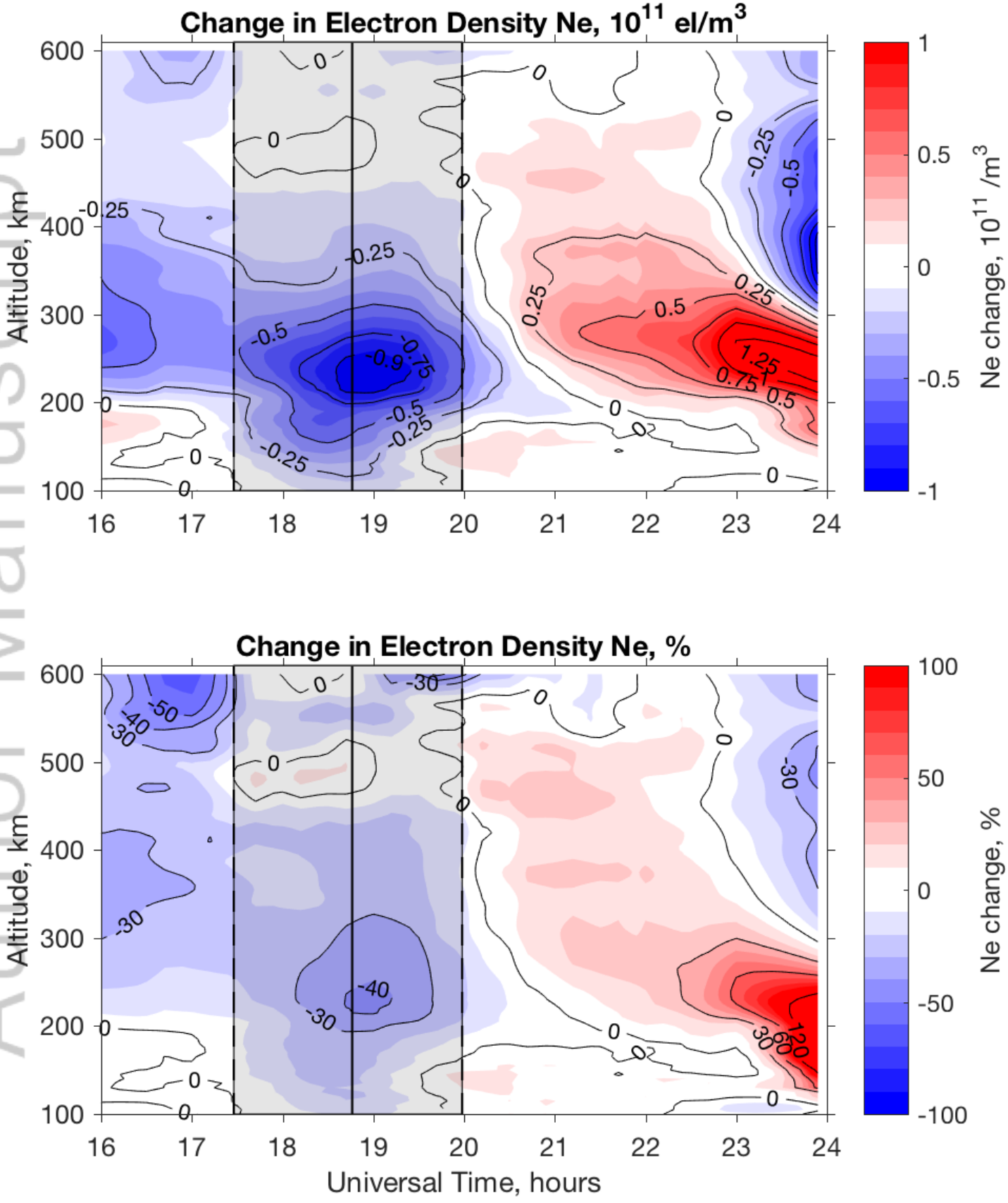

2018GL077334-f03-z-.png

This article is protected by copyright. All rights reserved.

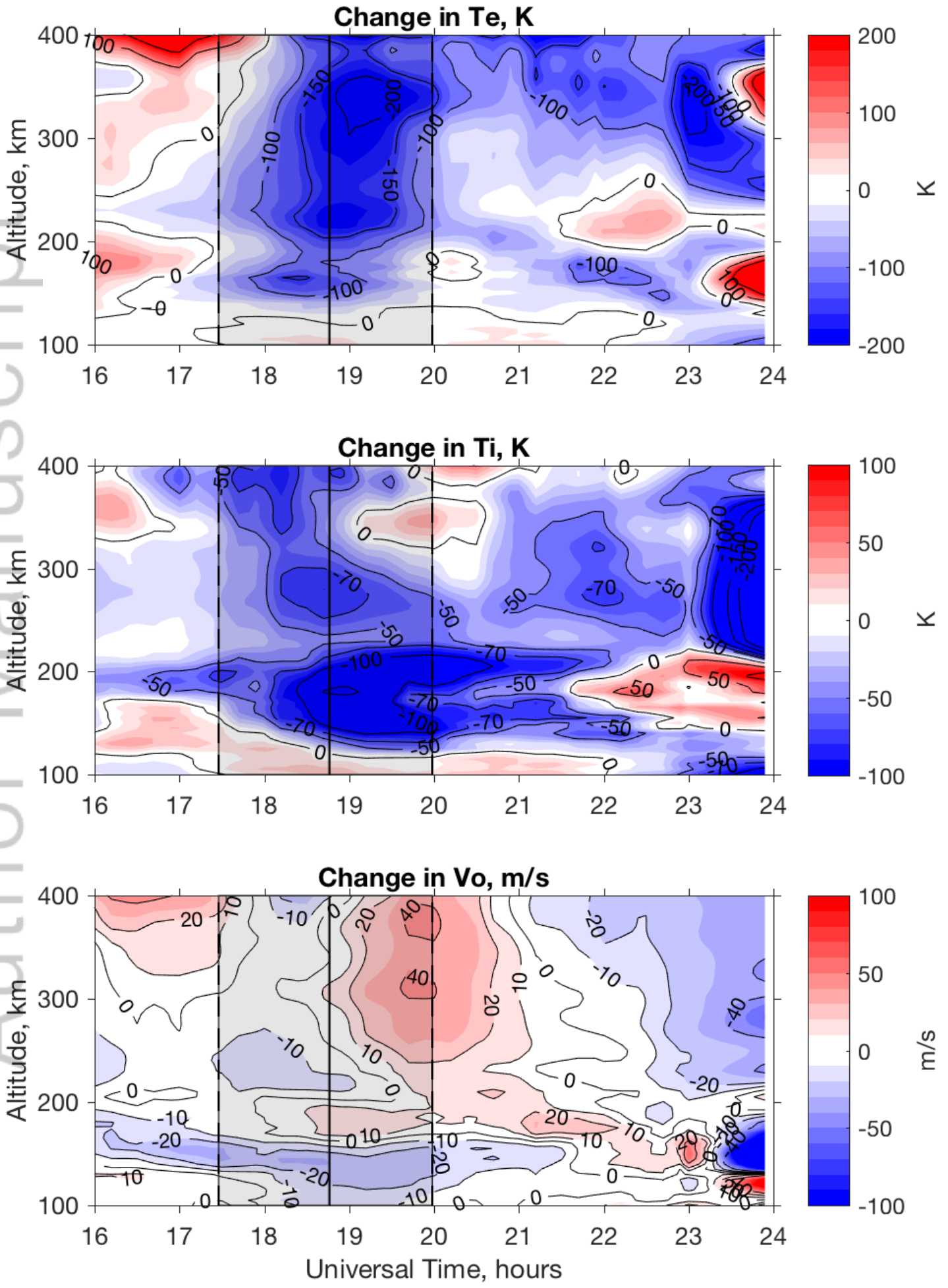

Author Manuscript

This article is protected by copyright. All rights reserved.

Author Manuscript

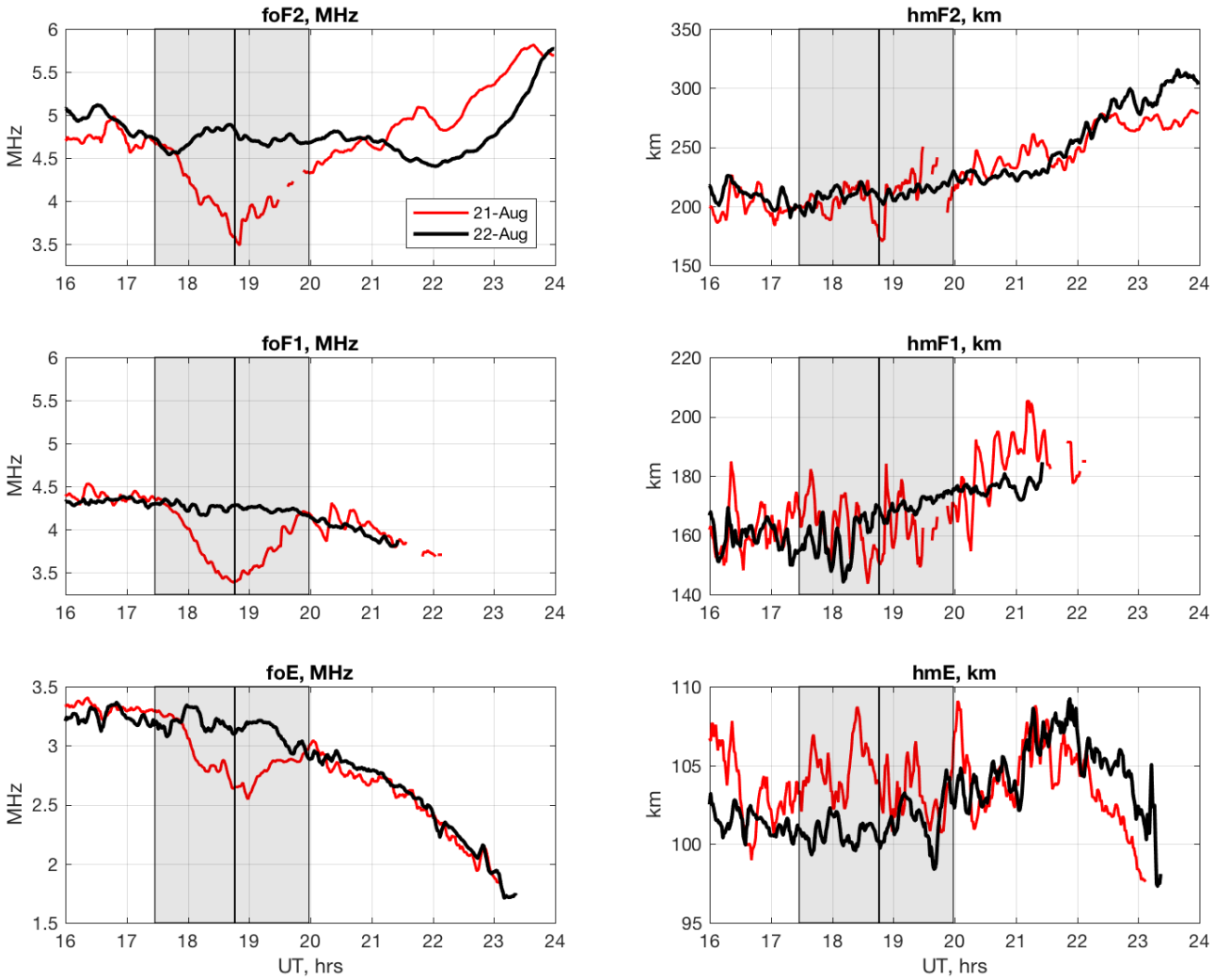

2018GL077334-f05-z-.png

This article is protected by copyright. All rights reserved.